26 May 2010, 5:30 pm - 5:40 pm

A Structural Engineer's Approach to Efficient SFSI: Towards Performance Based Design

M. Hesham El Naggar

The University of Western Ontario, Canada

Fifth International Conference on
Recent Advances in Geotechnical Earthquake Engineering and Soil Dynamics
and Symposium in Honor of Professor I.M. Idriss
May 24-29, 2010 • San Diego, California

A STRUCTURAL ENGINEER'S APPROACH TO EFFICIENT SFSI: TOWARDS PERFORMANCE BASED DESIGN

Prof. M. Hesham EL NAGGAR, Ph.D., P. Eng.
The University of Western Ontario
London Ontario, Canada N6A 5B9

ABSTRACT

Performance-based design (PBD) involves designing structures to achieve specified performance targets under specified levels of seismic hazard. This involves analyzing the entire soil-structure system and requires structural and geotechnical expertise. This paper is focused on soil-foundation-structure interaction (SFSI) in relation to PBD. A Beam-on-Nonlinear-Winkler- Foundation (BNWF) model is developed to incorporate important SFSI aspects into structural analysis software. The model accounts for: nonlinearity due to soil yield and/or footing uplift; cyclic degradation of stiffness and strength due to variable-amplitude loading; distribution of soil resistance underneath the footing for different loading conditions; reduction in radiation damping with increased nonlinearity; and coupling effects between different responses of the foundation. The coupling between different responses is achieved by appropriate mathematically derived bounding surfaces. The model utilizes a rotation hinge governed by a bounding surface to model coupling between rocking (in two directions) and vertical responses, and a shear hinge governed by another bounding surface to couple the horizontal responses. These models are implemented in readily available structural packages, and hence allow structural engineers to properly account for SSI effects when performing PBD. The application of the developed models to analysis of experiments on model foundations showed good agreement between the calculated and observed behavior.

INTRODUCTION

Structural response analysis has evolved into sophisticated techniques, and direct full-blown nonlinear building-soil response analysis is used nowadays more often. This evolution is enabled by advances in computing technology and efficient computational tools. Most of the insights gained from extensive analyses employing these computational tools are incorporated in modern seismic design codes to provide efficient and safe seismic design for buildings.

The traditional seismic design of structures follows the force-based design (FBD) approach, which intends to provide favourable dynamic response and avoid premature collapse. Seismic forces are calculated considering the estimated fundamental period and total mass of the structure with due consideration of the seismic hazard defined in terms of a design spectral acceleration. Lessons learnt from recent earthquakes have shown that although the basic intent of the code to provide life safety was achieved, damage to structures was extensive, leading to large economic losses and high cost of repairs (Eguchi et al., 1998). The performance-based design (PBD) approach, on the other hand, provides a more general design philosophy that seeks to achieve specified performance targets under stated levels of seismic hazard. To provide a specified performance at reasonable cost, accurate reliable analysis of the entire structure-foundation-soil system is important. Thus, the design approach relies heavily on nonlinear static and dynamic forms of analysis. Since the response analysis involves the entire system, robust and efficient analysis tools amenable for use by both structural and geotechnical engineers are required (Allotey and El Naggar, 2005a).

The advent of the PBD philosophy has renewed the need to revisit simplified modeling approaches, with the aim of developing robust and efficient analysis tools for modeling SSI problems. In addition, rigid body building failures in recent earthquakes (1985 Michoacan-Guerero earthquake in Mexico, Auvinet and Mendoza 1986; 1999 Kocaeli earthquake in Turkey, Gazetas 2001) highlighted the importance of incorporating SFSI into seismic designs. This is further corroborated by insights gained from design case

studies and earthquake damage distribution studies (Comartin et al. 1996; Trifunac and Todorovska 1999).

Dynamic SSI is a complex phenomenon that encompasses different types of response covering a range of sophistication in the analysis from a linear structure/soil to a nonlinear structure/soil. The nonlinearity stems from either material nonlinearity such as yielding of the soil or structure and cyclic strength/stiffness degradation of soil or structure; or geometric nonlinearity such as large displacements and foundation uplift. SSI is often assumed to have beneficial effects on seismic response. This may be attributed to the format of design spectra in most current design codes (Mylonakis and Gazetas, 2001). However, observations from recent earthquakes have highlighted the importance of performing realistic SSI analysis (Celebi and Crouse, 2001). In addition, PBD requires buildings to be designed to meet specific performance targets, which can only be achieved by ensuring that important factors that affect building response are properly accounted for.

The procedures used for soil modeling range from soil continuum approaches (e.g. finite element (FE) and boundary element (BE) formulations) to effective spring models (e.g. the macro-element approach and the beam-on-a-nonlinear Winkler foundation (BNWF) method). Although increases in computational power have reduced the time required for the FE and BE approaches, they remain generally unattractive to structural design engineers. The macro-element approach (Paolucci, 1997; Cremer et al., 2001; Houlsby and Cassidy, 2002; Gajan et al., 2005; and Chatzigogos et al., 2009) is able to satisfactorily predict the complete foundation response because it accounts for nonlinear behavior and coupling between the responses in all directions. However, the available macro-element models are based on specified bounding surfaces that may not be applicable to a wide range of problems.

The BNWF approach is widely used for predicting the nonlinear static response of SSI problems. The main drawback of the BNWF approach is using discrete decoupled springs to represent soil reactions at different points. For seismic applications, the static BNWF approach suffers two more disadvantages: its inability to account for the cycle-by-cycle SSI response; and its unsatisfactory performance in modeling problems involving significant kinematic interaction and ground motion effects (Finn, 2005). These factors can, however, be accounted for by using dynamic BNWF models. The use of dynamic BNWF has been mostly focused on soil-pile-structure interaction (SPSI) problems (e.g., Boulanger et al. 1999; El Naggar and Bentley, 2000; Gerolymos and Gazetas 2005; El Naggar et al., 2005).

The seismic response of shallow foundations is generally nonlinear and involves horizontal displacement, settlement and rocking, dissipating a considerable amount of the seismic energy. The BNWF model has been used for modeling some soil-footing-structure interaction (SFSI) problems such as linear or nonlinear rocking response of foundations (e.g. Psycharis and Jennings, 1984; Chopra and Yim, 1984; Filiatrault et al. 1992; and Anderson (2003). Nonetheless, it has the potential to simulate the most important phenomena of SSI including footing yield and uplift conditions, settlement and horizontal displacement and energy dissipation through hysteretic and radiation damping.

Allotey and El Naggar (2003, 2008a, 2008b) and El-Ganainy and El Naggar (2009) developed nonlinear Winkler models for the analysis of the total SFSI problem, i.e., for the analysis of the horizontal, vertical and rotational response modes. This follows the guidelines given in the National Earthquake Hazard Reduction Program (NEHRP) FEMA 273 & 274 documents (BSSC 1997) that recommends the nonlinear Winkler foundation approach for the analysis of SFSI problems. The main objectives of this paper are to: critically examine some important issues of SSI in PBD; and to briefly describe the developed models and use them to investigate some important aspects of SSI problems.

PERFORMANCE-BASED DESIGN

The objective of the FBD philosophy is to design buildings for life safety, and to minimize earthquake-induced damage to critical structures. The objective of PBD, on the other hand, is to design structures to achieve stated performance objectives when subjected to stated levels of seismic hazard (see Figure 1). The objective of FBD is achieved by specifying reduced levels of elastic strength through the force-reduction factor (R), and providing detailing for structural elements and connections to ensure a certain level of ductility. The performance targets in PBD are typically represented with deformation measures (Priestley, 2000). The outcome of PBD methodology is to provide building designs with a realistic and reliable understanding of their probable performance in future earthquakes, and for which quantitative measures such as risk of casualty, occupancy and economic loss are known. All variables that affect the seismic response of a structure must be adequately accounted for in order to accomplish a reliable PBD.

All PBD codes recommend the consideration of SSI in the design process (e.g. SEAOC Vision 2000 (SEAOC, 1995), ATC 40 (ATC, 1996) and FEMA 356 (ASCE, 2000) with its addendum FEMA 440 (FEMA, 2004)). The Pacific Earthquake Engineering Research Center (PEER) has developed a framework methodology for performance-based earthquake engineering (PBEE). The methodology is formulated probabilistically as:

$$\upsilon(DV) = \iiint G(DV/DM)dG(DM/EDP)dG(EDP/IM)d\upsilon(IM) \qquad (1)$$

where DV, DM, EDP and IM are the decision variable, damage measure, engineering demand parameter and intensity measure, which characterize the important aspects of the problem (Moehle and Deierlein, 2004). The geotechnical

aspects are accounted for in the term $dG(EDP/IM)$, and involves the analysis of the entire soil-structure system considering the direct approach for SSI. For the substructure approach, $dG(EDP/IM)$ can be expressed in terms of its sub-components as (Kramer and Elgamal, 2001):

$$dG(EDP/IM) = \iint dG(EDP/FIM)dG(FIM/FF)dG(FF/IM) \qquad (2)$$

where, $dG(EDP/FIM)$, $dG(FIM/FF)$, $dG(FF/IM)$ represent the contributions related to structural, soil-structure and site response analyses, respectively. To obtain reliable estimates of $dG(EDP/FIM)$, all three types of analysis must be treated with the same level of rigor. Thus, proper SSI analysis is as important as structural analysis, and is necessary for reliable designs.

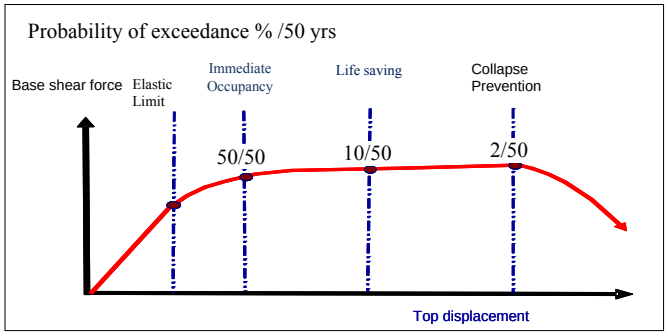

Figure 1: Capacity curve

Important SSI Issues in PBD

SSI Computational Tools: Most of existing programs are developed mainly for the analysis of the superstructure or the substructure. Geotechnically focussed programs use sophisticated soil models but over-simplified structural representation (Fig. 2a), while structurally oriented codes incorporate elaborate models for the structure, with a simplified representation of the soil (Fig. 2b). For example, commercially available structural analysis programs like SAP2000 (CSI, 2004), DRAIN-2DX (Prakash et al., 1993), RUAUMOKO (Carr, 2001), CANNY (Li, 2002) and SEISMOSTRUCT (SeismoSoft, 2003) are capable of modeling the structure well, but do not account for many important aspects of soil behaviour. On the other hand, geotechnical programs like FLAC (HCItasca, 2001) and SASSI2000 (SASSI2000, 1999) are capable of modeling geotechnical aspects, however, their structural features are relatively overly simplified. A stark example of this is the application of FLAC to study the cyclic response of a foundation (Pender and Ni, 2004), but the use of RUAUMOKO to study the nonlinear SSI response of a multi-storey building (Wotherspoon et al., 2004) in companion studies. The OPENSEES computational platform (PEER, 2000) is unique in that it offers an integrated environment for complete soil-structure system analysis, as it is developed from both points of view. More programs with this spirit are needed to further promote PBD.

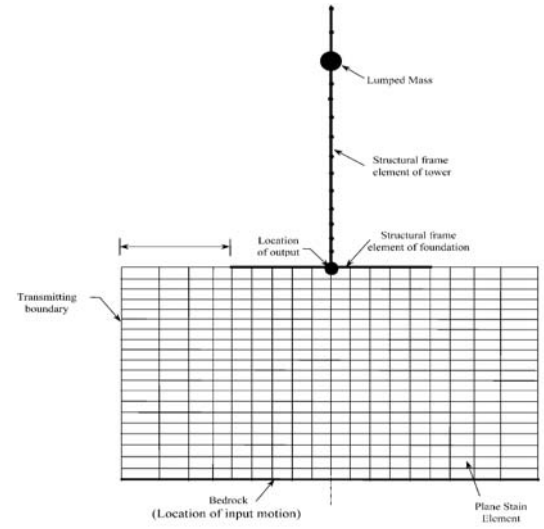

a)

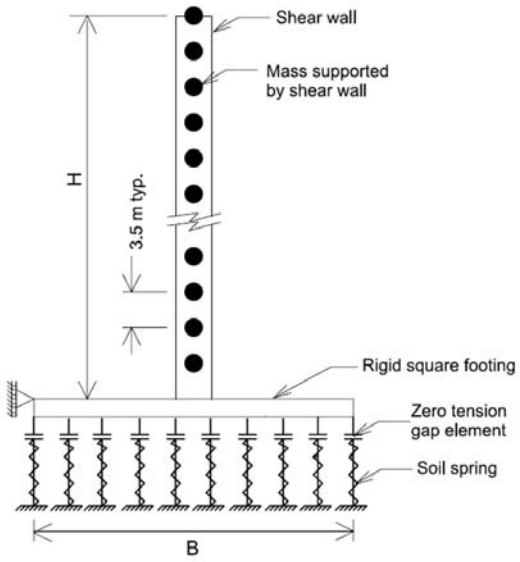

b)

Figure 2: Modeling of SSI, a) Geotechnical; b) Structural

The BNWF formulations that incorporate uplift capability implemented in some structural programs, allow for reasonable assessment of SSI effects on structures. However, they cannot adequately predict maximum cyclic displacements and permanent settlements as they do not account for cyclic soil degradation effects. These effects can impact the seismic response of buildings as observed in the 1999 Koaceli earthquake (Gazetas, 2001), and therefore should be incorporated into the BNWF models to improve their SSI capabilities.

SSI System Ductility (μ_s): There are conflicting views about the significance of the SSI system ductility parameter, μ_s, in the literature. Priestley and Park (1987) derived an expression for μ_s by assuming a bilinear elastic-force-displacement

relationship for the structure, and equivalent linear stiffness for the foundation, i.e.,

$$\mu_s = \frac{c_m + \mu_\Delta}{c_m + 1} \tag{3}$$

In Eq. (3), μ_Δ, is the structural ductility and c_m is the ratio of the contribution of mass displacement due to foundation motion to that of yield displacement of the structure. Based on their derivation, Priestley and Park (1987) argued that foundation compliance decreases the ductility capacity of a structure (also Priestley, 2000; Calvi, 2004). However, Gazetas and Mylonakis (2001) showed that μ_s is not a measure of the structural distress, rather it is a mathematical parameter that does not have any clear practical significance. Meanwhile, Aviles and Perez-Rocha (2003) derived an expression for the effective ductility of a nonlinear fixed-based oscillator equivalent to the SSI system by equating yield strength and ductility, i.e.

$$\mu_s = \frac{T^2}{T_s^2}(\mu_\Delta - 1) + 1 \tag{4}$$

where T and T_s are the periods of the fixed-base structure and SSI system. It can be shown that Eq. (3) is the same as Eq. (4), meaning that μ_s is the ductility of a fixed-base nonlinear replacement oscillator that would give the same response as the SSI system. Hence, μ_s cannot be linked to the ductility capacity of the structure.

Effect of Period-Lengthening: Traditional codes use design response spectrum approaches, which account for SSI effects by using the first mode period-lengthening ratio in combination with an estimate of the system damping (Stewart et al., 2003). With the exception of very short period structures, accounting for SSI in this approach results in reduced base shear forces (e.g. see Figure 3). This reduction contributes to the widely held belief that the effects of SSI on the seismic response of structures are favourable, and hence, there is no need to account for SSI in the case of non-weakening soils. Though this may be true for many structures, it is an overly simplistic view, and as noted by Gazetas and Mylonakis (2001), has the effect of crippling design innovation, and blinding the analyst to important SSI response features.

Gazetas and Mylonakis (2001) and Aviles and Perez-Rocha (2003) studied the response of yielding structures founded on soft soil. Ground motions at such soft soil sites (and sites in the normal forward fault-rapture direction of near-fault earthquakes, Somerville, 1998) are usually characterized by long predominant periods. For such cases, period-lengthening for structures with fixed based periods less than the predominant period can result in a resonance condition, resulting in higher forces and ductility for the flexible base system in comparison with the fixed-base case. Their results indicate that period lengthening for yielding structures is a result of the effects of SSI and structural degradation, and the interaction between these variables makes it difficult to assess with certainty whether SSI will be beneficial or not. Due to the possibility of period-lengthening causing resonance, it is important that every structure with periods shorter than the predominant site period be assessed to check if this condition would be of concern. In addition, site-specific response spectra should be developed to minimize the averaging effects inherent in traditional code design spectra. In the context of PBD, this is important since unsatisfactory input intensity measures (*IM*) directly impact the output decision variable (*DV*).

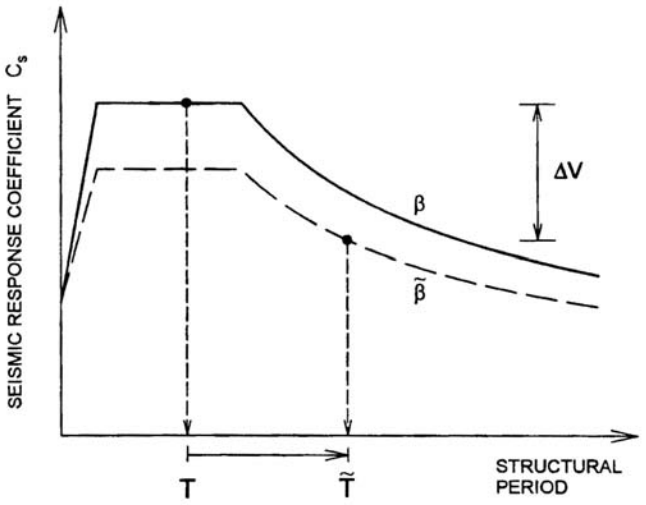

Figure 3 Reduction in design base shear due to SSI according to NEHRP-97 seismic code

Foundation Stiffness, Bearing Capacity and Coupling Effects: Since nonlinearity can only be accounted for in a time-domain analysis, frequency-independent foundation stiffness values are usually used in nonlinear SSI analysis. The frequency-independent stiffness is typically calculated assuming some idealized soil profiles (Gazetas, 1991). Because SSI effects can be site-specific due to resonance and de-resonance features, stiffness values representative of the actual site conditions should be used in the analysis. Site-specific stiffness can be evaluated using FE and BE techniques, however, this may be tedious and time consuming. Alternatively, foundation stiffness, and its bearing capacity (BC) can be determined from tests such as: plate load tests, consolidation tests, triaxial tests, etc.

The FEMA 356 (ASCE, 2000) design guideline recommends foundation stiffness to be estimated considering half-space solutions, with a corresponding appropriate value of the medium shear modulus. It also recommends the estimation of the BC under concentric vertical load with standard BC formulae (e.g. Vesic, 1973). To account for soil parameters variability, the guideline recommends that the estimates of stiffness and strength be varied between an upper and a lower bound of two-times and half of the best-estimate, respectively. For FS < 2, lower bound strengths could be less than the imposed static pressure and the recommendation cannot be followed directly.

Recent approximate methods such as the cone model approach by Wolf and Preisig (2003) and Wolf and Deeks (2004), and the differential cell method by Nogami and Chen (2004) can be used to obtain the stiffness of footings resting on uniform and layered soil profiles. These approaches are easy to implement, and with the availability of mathematical software (e.g.Mathcad and Matlab), it is possible to obtain representative stiffness values for any site and to perform sensitivity analyses, which could be very useful in achieving efficient and reliable design (Crouse and McGuire 2000). Programs like DYNA5 (El Naggar et al., 2007) can be used to calculate the stiffness of foundations resting on different soil conditions. The availability of these tools facilitates proper evaluation of foundation stiffness and thus more accurate SSI.

The stiffness and BC of rigid footings depend on the stress distribution under both working and ultimate load conditions. The stress distribution underneath a foundation is difficult to predict accurately, and depends on factors such as soil type, depth of footing and load level. Theoretical elastic solutions predict a convex parabolic stress distribution with infinite edge stresses, which in practice are finite due to local yielding (Shultze, 1961). Under ultimate loading conditions, plastic solutions predict a linear-to-concave parabolic distribution of stress (Kerr, 1989). The stress distribution under low load levels is primarily influenced by the edge stress, which depends on the soil type and footing depth. Generally, as the load increases, the distribution becomes less convex and more concave. The stiffness and BC can vary significantly as some or all these factors vary, and therefore, Allotey and El Naggar (2007) developed stiffness and BC distribution functions for rectangular footings accounting for the footing aspect ratio, edge stress and curve shape factors.

The main drawback of the BNWF approach is its idealization of the soil continuum with discrete soil reactions at different points that are decoupled from each other. In most models, the soil reactions along the different degrees of freedom are also decoupled. This drawback is addressed in the models presented in this paper.

Cyclic Degradation Effects: Cyclic degradation is directly accounted for in coupled BNWF models by using an effective stress formulation. On the other hand, most uncoupled models do not account for cyclic degradation. A few uncoupled BNWF models account for cyclic degradation for constant-amplitude loading conditions. For example, Bouc-Wen models employ parameters that are a function of the dissipated hysteretic energy or the cumulative displacement ductility to account for cyclic degradation (Gerolymos and Gazetas, 2005). Other uncoupled models account for it by using stiffness and/or strength modification factors to degrade force-displacement curves. Idriss et al. (1978) developed a combined stiffness-strength degradation approach and introduced a hyperbolic force-displacement curve and an expression for its modification factor, i.e.

$$p(y) = \frac{y}{\frac{1}{K_0} + \frac{y}{p_f}} \tag{5}$$

$$\delta_y\left(y_n\right) = \frac{\delta_k \delta_t \left(1 + y_n\right)}{\left(\delta_t + \delta_k y_n\right)} \tag{6}$$

where δ_y is the degradation factor at normalized displacement $y_n = y/y_r$, $y_r = p_f/K_0$ is the reference displacement and δ_k and δ_t are the stiffness and strength degradation factors. Stiffness-only or strength-only modification behaviour can be modeled using Eq. 6 by setting $\delta_t = 1$ and $\delta_k = 1$, respectively. For stiffness-only and strength-only methods, the shape of the backbone curve is not preserved through the degradation process. The combined stiffness-strength approach, on the other hand, preserves the shape for the case when $\delta_k = \delta_t$.

Modeling Energy Dissipation: The soil damping provides a major source of energy dissipation in soil-foundation systems subjected to dynamic loading. There are two different types of damping that should be considered in seismic SFSI problems, namely radiation and material damping. Usually, radiation (geometric) damping is most important in the far field while material (hysteretic) damping provides most energy dissipation in the near field. Radiation damping is due to wave propagation away from the foundation, and is directly related to the soil compression and shear wave velocities. Hysteretic damping is caused by the plasticity of the soil and possibly discontinuity conditions (uplift and/or sliding) at the foundation-soil interface.

Foundation Input Motion: Foundation input motion (FIM), i.e., motion experienced by the foundation due to interaction with the free-field motion, represents another challenge in SSI modeling. Due to lack of data and poor analysis procedures, kinematic interaction effects have mostly been neglected in SSI substructure analysis. However, the measured response of several buildings with basement portions during the Kobe earthquake (Iguchi, 2001) showed that there can be a considerable difference between the FIM and free-field motion, which underscores the importance of the accurate prediction of the FIM in PBD.

Two simple methods are available for evaluating FIM: Kim and Stewart (2003) for surface foundations; and Kurimoto and Iguchi (1995) for both surface and embedded foundations. Kurimoto and Iguchi evaluate the weighted-average of free-field displacements along the soil-foundation interface and add the displacements caused by the resultant force and moment associated with the free-field tractions along the interface. This procedure can be implemented in Mathcad or Matlab to evaluate the FIM, using footing impedance functions.

FOUNDATION RESPONSE CHARACTERISTICS AND ITS MODELING

General Response Behavior

During a seismic event, a footing would go through vertical, lateral and rotational displacements due the seismic vertical, horizontal and moment loading as shown in Fig. 4a. If movement in any of these directions exceeds an acceptable threshold, the foundation is deemed to have failed. Figure 4b shows two possible failure mechanisms: failure due to the formation of an asymmetric slip surface associated with rotation about footing right edge under pure moment loading; and failure due to formation of an asymmetric slip surface associated with rotation about footing left edge under pure horizontal loading. The slip surface is typically shallow for the horizontal case and deep under rocking motion, and is typically skewed due to uplift. In either case, the SFSI response is generally characterized by a beneficial reduction in structural loads and an increase in energy dissipation, associated with the development of permanent deformation. Permanent deformations can be detrimental and must be controlled. In particular, permanent rotations can significantly affect the SFSI response (Zeng and Steedman, 1998; Maugeri et al., 2000).

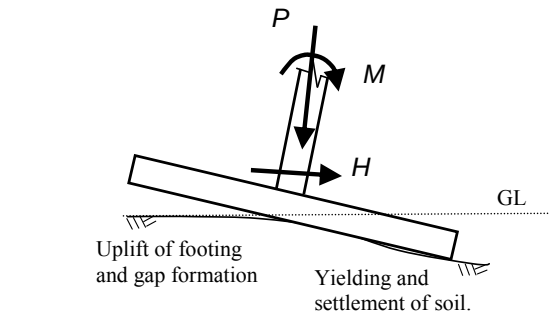

a)

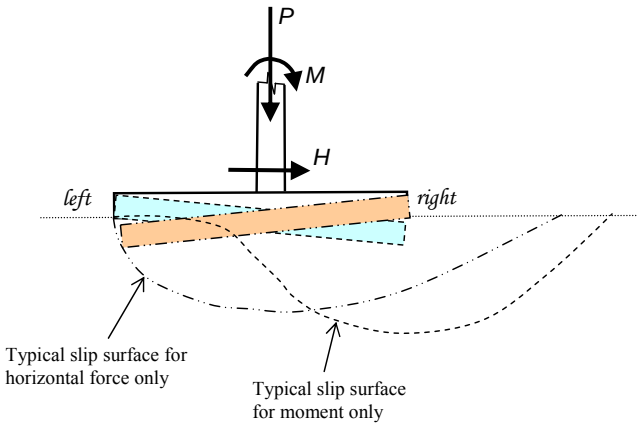

b)

Figure 4: a) Schematic of foundation under horizontal and vertical forces and moment actions; b) Asymmetric failure surfaces due to horizontal force-only and moment-only actions

FEMA Recommended Modeling Technique

The FEMA 356 (ASCE, 2000) guidelines recommend that foundations can be modeled as shown in Fig. 5. The horizontal response (modeled with an independent horizontal spring) is uncoupled from the vertical-rotational responses (modeled with distributed vertical springs). The guidelines recommend foundation stiffness to be estimated considering half-space solutions, with an appropriate value of the shear modulus. They also recommend the estimation of the BC under concentric vertical load with standard BC formulae (e.g., Vesic, 1973). To account for soil parameters variability, the guidelines recommend varying the estimates of stiffness and strength between upper and lower bounds of two-times and half of the best-estimate, respectively. The stiffness and BC of rigid footings can vary significantly depending on the shape of the footing and the stress distribution under both working and ultimate load conditions, respectively. For a building with an embedded foundation (which is mostly the case), the effects of footing embedment, such as the passive pressure mobilized at the toe of the footing leading to reduced horizontal sliding, should be considered.

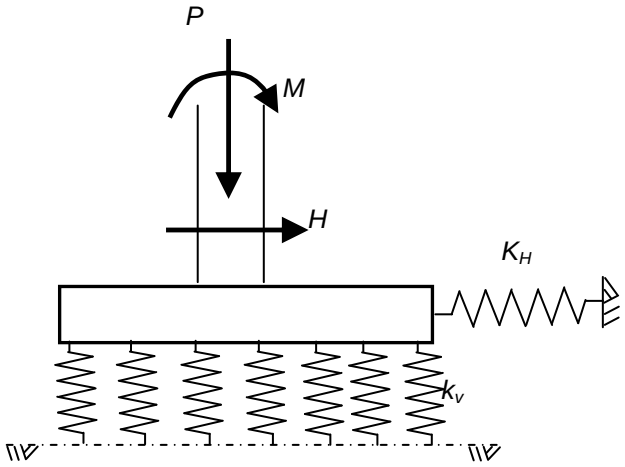

Figure 5 schematic of recommended FEMA 273/274 Winkler modeling approach

GENERALIZED DYNAMIC BNWF MODEL

Allotey and El Naggar (2003) developed analytical formulae to represent the moment-rotation behavior of rigid footings, categorized as uplift-dominant, yield-dominant or uplift-yield categories. This backbone moment-rotation curve can be characterized by two dimensionless quantities, $\chi = P/P_u$ and $\psi = k_v(2a)^2/P_u{:}\chi$ controls the moment capacity, and ψ, the shape of the curve. P and P_u are the imposed and ultimate

vertical loads, k_v is the subgrade modulus and $2a$ is the side length of a $2a$ x $2b$ rectangular footings. χ is the inverse of the factor of safety (FS) under concentric vertical load and represents the closeness of the imposed static pressure to yield pressure. As such, the nonlinear Winkler model with uniform distribution of stiffness and bearing capacity (BC) predicts χ = 0.5 as the condition of maximum moment (Allotey and El Naggar, 2003). Values between 0.4 - 0.5 have been obtained in various experimental and finite element studies (e.g., Pecker, 1997; Cassidy et al., 2004).

To account for footing cyclic degradation/hardening behavior, Allotey and El Naggar (2008a) developed a generalized cyclic normal force-displacement model to be used in the context of BNWF. The model is multi-linear with defined rules for loading, unloading and reloading. The model can be classified as a degrading polygonal hysteretic model and can be used for simulating response of retaining walls, shallow foundations and piles (two elements are needed at each level for a pile foundation). This model is described below.

Backbone Curve

The backbone curve comprises a four-segment adaptable multi-linear curve (i.e., segments 1, 2, 3 and 4 in Fig. 6a) that can represent two types of behavior: monotonic response (represented by solid lines in Fig. 6a), where the four segments simulate the curve from start to failure; and post-peak residual behavior, where segments 1 and 2 are used to model the curve up to the peak force, after which segments 3 and 4 (represented by dotted lines in Fig. 6a) are used to model the post-peak behavior. The descending branch of the backbone curve acts as a strength cap superimposed on the "true" monotonic response, and relates the current strength to the maximum displacement. The parameters needed to establish the backbone curve (p_0-p_3, y_0-y_3, α_1-α_3) can be evaluated from specified force-displacement (or p-y curves) using curve-fitting methods.

Standard Reload Curve and General Unload Curve

Figure 6b shows an example of the reloading curve termed the standard reload curve (SRC), and the unloading curve, termed the general unload curve (GUC). These curves are derived from the backbone curve similar to the models based on extended Masing rules. However, the scaling factor is estimated accounting for strength degradation, i.e.,

$$\kappa = 1 \pm \frac{p_{ur}}{\delta_t p_f} \quad \text{"+": unloading; "-": reloading} \qquad (7)$$

For monotonic backbone curves, the SRC is comprised of four segments, i.e., 7-8-9-10; for backbone curves exhibiting a post-peak behavior, segments 9 and 10 are merged and the SRC is comprised of only three segments. The expressions for the coordinates of the nodal point (p'_i, y'_i) of a degraded multi-linear curve can be derived as:

$$\left(p'_i = \sum_{i=1}^{j} \delta_t (p_i - p_{i-1}),\ y'_i = \sum_{i=1}^{j} \frac{\delta_t (y_i - y_{i-1})}{\delta_k} \right) \quad j = \max(i) \forall y_i \le y, j \ge 0 \qquad (8)$$

Figure 6b shows equations for the various nodes of the SRC (p_{r1}, y_{r1}; p_{r2}, y_{r2}; p_{r3}, y_{r3}) and GUC (p_{u1}, y_{u1}). When the SRC crosses the initial backbone curve, two options exist: to follow the original backbone curve, similar to extended Masing rules; or to continue along the SRC (i.e., for hardening conditions).

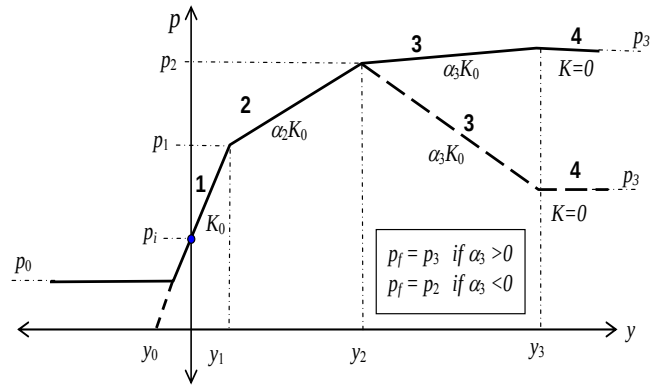

a)

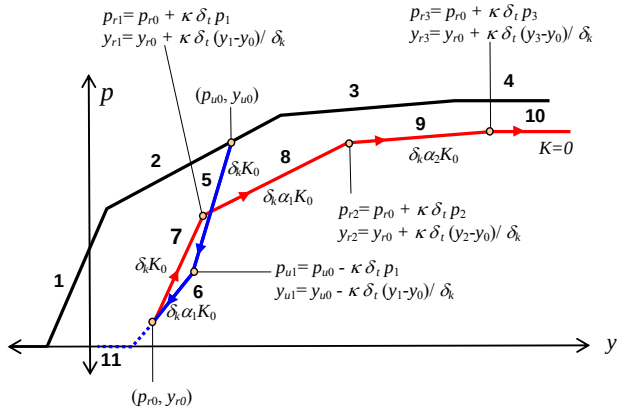

b)

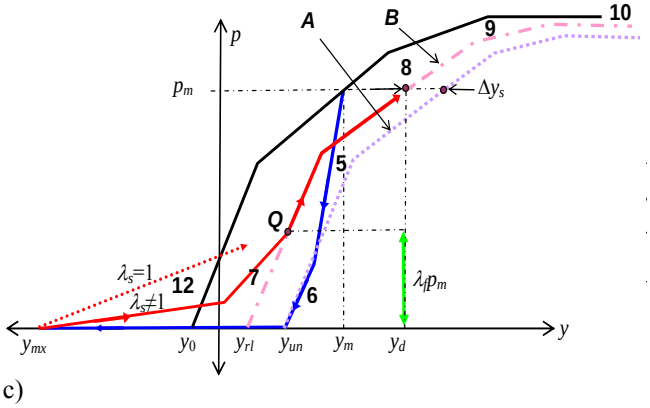

c)

Figure 6: Schematics of: a) backbone curve; b) standard reload and general unload curves; c) direct reload curve

Direct Reload Curve

The direct reload curve (DRC) simulates soil reactions to a foundation moving in the slack zone. It starts immediately after movement at the minimum force level in the negative direction. The DRC is designed as a convex strain-hardening curve, controlled by a limiting force parameter λ_f ($0 \le \lambda_f \le 1$) that is referenced to the past maximum force, and a curve shape parameter, λ_s, ($0 \le \lambda_s \le 1$) to control the shape of the DRC. The parameters λ_f and λ_s together control the shape of the hysteresis loops formed. For a fully unconfined response - pure gap -, $\lambda_f = 0$ or $\lambda_s = 0$, and for a fully confined response, $\lambda_f = \lambda_s = 1$. Both parameters vary between 0 and 1 with soil type and depth, based on expected amount of soil cave-in and dilatancy effects.

A limiting strain parameter is necessary to model strain-hardening (Elgamal et al. 2002). In Fig. 6c, curve *A* represents the SRC for a foundation that moves back to meet the soil at the point where it separated, accounting for gap closing before reloading in stiff clay soils. Curve *B* is offset from curve *A* to the left by Δy_s; this offset increases with the magnitude of soil cave-in. An expression for the origin of the current base-SRC was developed using a large dataset of one-way, two-way and intermediate constant cyclic load tests on piles in sand, compiled by Long and Vanneste (1994). Based on their study, the origin of the current base-SRC, y_{rl}, could be derived:

$$y_{rl} = y_0 + h_L \left(y_{un} - y_0 \right) \tag{9a}$$

$$h_L = \frac{1}{1 - \Lambda \phi_h} \tag{9b}$$

$$\phi_h = \frac{y_{mx} - y_{un}}{y_m + y_{un} - 2y_0} \tag{9c}$$

In Eq. (9), h_L is a hyperbolic function that depends on the soil cave-in parameter, Λ ($\Lambda \ge 0$), and the cyclic loading ratio, ϕ_h (i.e., maximum distance moved at the minimum force level divided by the displacement for two-way loading). The range - $1 \le \phi_h \le 0$, and $\phi_h = -1$ represents two-way loading, and $\phi_h = 0$ represents one-way loading. Also, y_{mx} is the current maximum displacement at the minimum force level, y_m is the displacement corresponding to two-way cyclic loading, y_{un} is the current "most-right" unload displacement at the minimum force level and y_0 is the origin of the backbone curve.

Modeling of Cyclic Degradation

A modified version of Anthes (1997) rainflow counting technique is developed based on forming "virtual" half-cycle loops and later identifying full-cycle loops. The algorithm calculates current cumulative damage, *D,* accounting for the number of equivalent loading cycles. The incremental damage, ΔD, for the current half-cycle loop is evaluated as (Allotey and El Naggar, 2008c):

$$\Delta D_{j,j-1} = \frac{1}{2N_f(S_i)} \tag{10}$$
$$S_i = S_{r_j} - S_{r_{j-1}}$$

where, N_f is the number of cycles to failure at a cyclic force (stress) ratio of S_i (taken as a ratio of the soil strength), and S_{r_j} and $S_{r_{j-1}}$ are the beginning and ending force ratios for the current half-cycle loop. N_f is obtained from the failure condition curve (e.g., *S-N* curve from cyclic triaxial or simple shear tests). It is defined by the cyclic force (stress) ratio at $N = 1$, S_1, and the negative slope of the failure condition line, η_{SN}. There are two possible forms of the failure condition curve: log-log model (Sharma and Fahey 2003); and semi-log model (Hyodo et al. 1994). A stress-independent elliptical degradation function (Allotey and El Naggar 2006), is used to evaluate the stiffness and strength degradation factors, i.e.,

$$\delta_\varsigma = 1 + \left(\delta_{m\varsigma} - 1 \right) \left[1 - \left(1 - D \right)^{\theta_\varsigma} \right]^{\frac{1}{\theta_\varsigma}} \tag{11}$$

where, ς stands for *k* or *t* (for stiffness and strength degradation factors, δ_k and δ_t, respectively), $\delta_{m\varsigma}$ is the minimum/maximum amount of degradation and θ_ς, is the curve shape parameter. Table 1 shows typical ranges for the degradation model parameters.

Table 1:Typical range of degradation parameters assuming free-field degradation

Parameter	Range	Reference
Saturated sand		
η_{SN}	0.3-0.4	De Alba et al. (1976), Popescu and Prevost (1993)
S_1	0.8-1.2	De Alba et al. (1976), Popescu and Prevost (1993)
θ_k=θ_t	0.7-1.1	De Alba et al. (1976)
Undrained clay		
η_{SN}	0.07-0.15	Hyodo et al. (1994); Andersen et al. (1988)
S_1	1	Hyodo et al. (1994); Andersen et al. (1988)
θ_k	1.5-2.5	Vucetic and Dobry (1988)*
θ_t	0.75-0.95	Carter et al. (1982)*

* Evaluated from data available in Reference

Modeling Damping

Radiation Damping: Radiation damping is modeled using a stiffness-proportional nonlinear damping formulation that comprises a nonlinear dashpot placed in parallel with the

nonlinear spring. This is an adaptation and extension of the approach used by Badoni and Makris (1996). The damping constant at each time is related to the current stiffness; with the small-strain initial value estimated using impedance functions available in the literature (e.g., Novak et al. (1978); Gazetas and Dobry (1984)). The proposed damping model is given by:

$$p_d = \left[c(a_o)\alpha_{i\_t} \right] \dot{y} \quad \text{and} \quad c(a_o) = G_{\max} a_o S_{u2}(a_o, \upsilon_s) \qquad (12)$$

where S_{u2} is a dimensionless constant that is a function of the Poisson ratio, υ_s and the dimensionless frequency, $a_0 = \omega r / V_s$, where, ω is the circular frequency, V_s is the soil shear wave velocity, r is a characteristic dimension, G_{max} is the small-strain shear modulus, c is the initial damping constant, α_{i_t} is the current stiffness ratio, and p_d and $\dot{y}$ are the damping force and relative velocity, respectively.

Hysteretic Damping: The hysteretic damping ratio, ξ_h, of the model ranges from zero (for elastic response) to maximum energy dissipation per cycle under two-way cyclic loading (for $\lambda_f = \lambda_s = 1$):

$$\xi_h = \begin{cases} \dfrac{1}{2\pi}\left[2 - \dfrac{K_s}{K_0}\right] & \varphi \le \dfrac{\varphi_1}{1-\varphi_1} \\ \dfrac{1}{2\pi}\left[2 - \dfrac{K_s}{K_0} - \left(\dfrac{K_s}{K_0}\right)\left(1 - \dfrac{(1+\varphi)}{(\varphi/\varphi_1)}\right)^2 \left(\dfrac{1}{\alpha_1} - 1\right)\right] & \varphi > \dfrac{\varphi_1}{1-\varphi_1} \end{cases} \qquad (13)$$

where $\varphi_i = p_i/p_f$, K_s is the secant stiffness. It is noted that the maximum model damping ratio possible is $\xi_h = 1/\pi$. The damping ratios obtained with the model lie within the range of damping ratios obtained from various soil cyclic tests (Allotey and El Naggar 2008a).

COUPLED BNWF MODEL

A foundation can be incorporated in structural models as a hinge attached at the bottom of ground floor column. The moment capacity of this hinge would be limited to the moment capacity of the footing. The coupled BNWF model is a practical approach for simulating the 3D nonlinear response of shallow foundations to general cyclic loading. It utilizes the coupled P-M_2-M_3 hinges and coupled V_2-V_3 shear hinges available in most commercial structural analysis software (e.g. SAP2000 and Perform-3D). These hinges are mostly rigid-plastic hinges (i.e. they resemble rusty hinges, and cannot model elastic behavior).

The methodology involves replacing the Winkler foundation by an assemblage of a moment-rotation hinge and an elastic beam-column element. The mechanical and geometrical properties of this assemblage are calculated mathematically. Unlike the uncoupled BNWF approaches used in modeling vertical and rocking responses of shallow foundations, the analysis considers an appropriate bounding surface for the rotation hinge. The interaction between the footing moment capacities along its width and length is also incorporated in the model using a numerically calibrated bounding surface. Similarly, the footing 3D rocking and shear responses are coupled through approperiate bounding surfaces along its length and width.

Moment-Rotation Hinge

The seismic response of buildings involves two forms of rocking; local rocking of individual footings and global rocking of the whole building. Local rocking is usually modeled in the context of BNWF for footings employing moment-rotation relations involving bilinear representation: an initial elastic state segment and perfectly plastic segment defined by the ultimate moment capacity. The slope of the elastic segment represents the initial slope of the actual moment-rotation relation, and its ultimate moment capacity is limited to that of the footing moment-rotation, M_u. El Ganainy and El Naggar (2009) give the bilinear approximation of the moment-rotation relation for a rectangular footing in terms of its width (B) and length (L), i.e.

$$M = \frac{k_v B^3 L \theta}{12} \qquad (14a)$$

$$M_u = \frac{PB}{2} - \frac{P^2}{2 q_u L} \qquad (14b)$$

Where: P = applied vertical load; M = applied moment along footing width; θ = footing rotation along its width; k_v = soil subgrade modulus; q_u = footing ultimate bearing capacity.

This behavior can be reprodruced by connecting an elastic frame member in series with the moment-rotation hinge. The member length L_T (selected as minimum) and curvature stiffness EI should be calculated to give the desired initial slope for the bilinear moment-rotation relation, i.e.:

$$\frac{EI}{L_T} = \frac{k_v B^3 L}{12} \qquad (15)$$

P-M_B-M_L Bounding Surface

The global rocking varies the vertical loads acting on individual foundations. This variation could alter the moment capacity of these footings due to the interaction between the vertical load and the moment capacity of the footing.

Figure 7a shows the footing moment capacity, M_U and the vertical load, P, relation derived for a rectangular footing of width B and length L, which has uniform stiffness and bearing capacity distributions (El Ganainy and El Naggar, 2009). To

account for the interaction between the applied vertical load and the footing moment capacity using the moment-rotation hinge approach, an appropriate bounding surface is utilized.

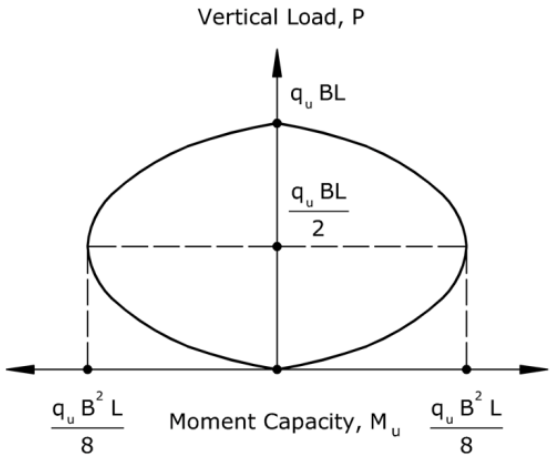

a)

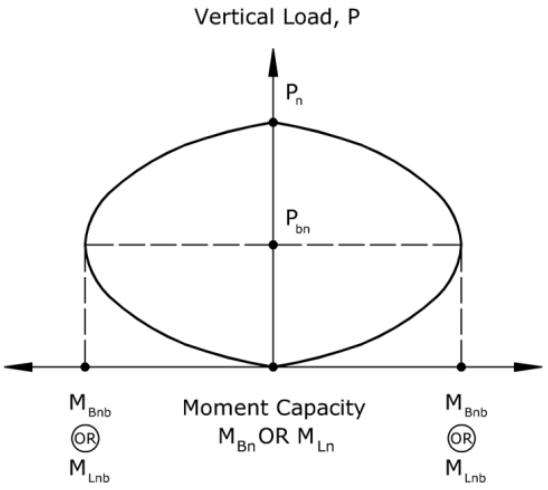

b)

Figure 7 a) Variation of moment capacity of rectangular footings with applied vertical load; b) P-M_u bounding surface

To completely define the bounding surface relating P to M_u along B and L, the interaction between P and M (for uniaxial moment loading) and interaction between the moment capacities of the footing along B and L (for biaxial moment loading) are defined. Decoupling the effect of horizontal loads at this stage, Figure 10a can be used to define the bounding surface that represents the interaction between P and M For a rectangular footing, the last curved segment of the moment-rotation curve corresponding to the uplift and yield condition can be represented by (El Ganainy and El Naggar, 2009):

$$M_u = \frac{B}{2}\left(P - \frac{P^2}{q_u BL}\right) \tag{16}$$

The bounding surface equations proposed by El-Tawil and Deierlein (2001) can be rewritten for rectangular footings in more compact form, i.e.:

$$\left(\frac{M_B}{M_{Bn,p}}\right)^n + \left(\frac{M_L}{M_{Ln,p}}\right)^n = 1.0 \tag{17a}$$

$$\frac{M_{Bn,p}}{M_{Bnb}} = \left(1 - \left(\frac{|P - P_{bn}|}{P_n - P_{bn}}\right)^2\right) \tag{17b}$$

$$\frac{M_{Ln,p}}{M_{Lnb}} = \left(1 - \left(\frac{|P - P_{bn}|}{P_n - P_{bn}}\right)^2\right) \tag{17c}$$

Where: M_B and M_L are moment capacities of the footing along B and L; $M_{Bn,p}$ and $M_{Ln,p}$ are footing moment capacities along B and L under vertical load P; M_{Bnb} and M_{Lnb} are the footing moment capacity along B and L at the balanced point; P_{bn} is vertical load at the balanced point; P_n is footing vertical load capacity; n is a fitting exponent that control the bounding surface shape in $(M_{Bn} - M_{Ln})$ plane. The bounding surface for the moment capacity-vertical load relation for rectangular footings described in Eq. 17 is shown in Figure 7b.

The bounding surface relating P and M_u in case of uniaxial moment loading is derived from Eqs. 16 and 17 (and calibrating Eq. 17a numerically for bounding surfaces of rectangular footings with different aspect ratios for bearing capacity factor of safety = 2) and is given by (El Ganainy and El Naggar, 2009):

$$\frac{M_u}{\left(q_u B^2 L/8\right)} + \left(\frac{P - \left(q_u BL/2\right)}{q_u BL/2}\right)^2 = 1 \tag{18}$$

The fiber cross-section approach (e.g. Perform-3D, Computers and Structures 2007) can be used to represent the footing behavior employing an inelastic frame element. The cross-section is discretized into independent fibers that can be of different materials. The soil properties are assigned to the fibers material, and the area properties (i.e. area and moment of inertia about both axes) of the fiber section as a whole are equal to the area properties of the modeled footing. Each material type is defined by its uniaxial stress-strain relationship, whereas the axial load and biaxial moments acting on the cross-section are applied at its centerline. The axial stress in each fiber is calculated using the stress-strain relationship for this fiber and its compression or extension. From a geotechnical prospective, the fiber section approach is similar to the BNWF approach as it can be seen as modeling

cross-sections using closely spaced discrete independent springs, each has a nonlinear force-deformation relationship.

The interaction between footing moment capacities along B and L, in case of biaxial moment loading was also investigated. The bounding surface for rectangular footings that describes the interaction between the moment capacities of the footing along its width, M_B, and length, M_L, in case of biaxial moment loading for BNWF model with uniform stiffness and bearing capacity distributions, can be expressed as (El Ganainy and El Naggar, 2009):

$$\left(\frac{M_B}{M_{Bn,p}}\right)^{1.8}+\left(\frac{M_L}{M_{Ln,p}}\right)^{1.8}=1.0 \qquad (19)$$

Using Eqs. 18 and 19, the complete P-M_B-M_L bounding surface for rectangular footings can be defined, assuming uniform stiffness and bearing capacity distributions. Figure 8 shows a schematic of the normalized bounding surface drawn in P-M_B-M_L space.

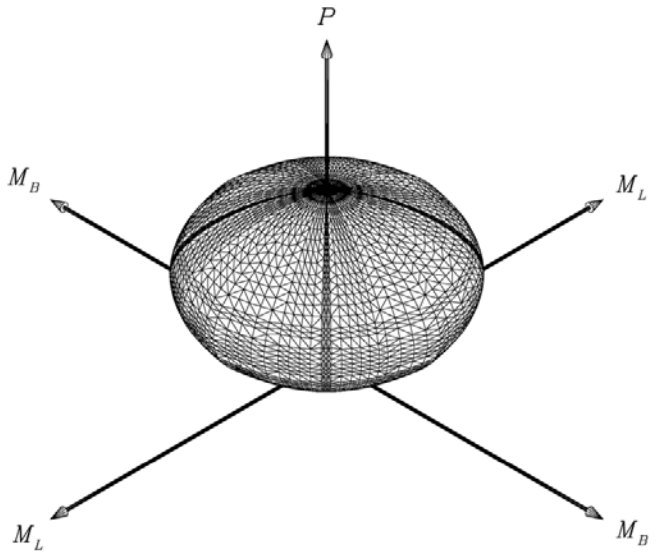

Figure 8. Schematic of normalized $P-M_B-M_L$ bounding surface for rectangular footings

V_B-V_L Shear Hinge

The footing horizontal capacity, F_u, assuming that the failure mode will be sliding at the footing-soil interface, arises from three components: base friction, which is the main resistance mechanism; soil passive resistance along the footing front face and side friction resulting from friction at the footing side-soil interface. FEMA 356 (2000) document provides guidelines for calculating the footing horizontal capacity components.

The coupled BNWF model utilizes shear hinges to model the horizontal force-displacement response of the supporting footings accounting for the footing elastic horizontal stiffness, its horizontal capacity and the inelastic energy dissipated in the hysteresis force-deformation action under cyclic loading. In the case of biaxial horizontal loading, an appropriate bounding surface is used to account for the interaction between the footing horizontal capacities along its width and length. An elastic frame member is connected in series with the shear hinge to account for elastic force-deformation action. Its length (L_T) and shear area (A_S) are calculated to give the desired initial slope for the footing horizontal force-deformation, , i.e.

$$\frac{GA_S}{L_T}=K_H \qquad (20)$$

where G is the shear modulus of foundation soil and K_H is its elastic horizontal stiffness.

A moment-rotation hinge and a shear hinge fully describe the behavior of footings accounting for moment-rotation and horizontal responses. Since both hinges comprise a rigid-plastic hinge and an elastic frame member connected in series, it is reasonable to use only one elastic frame member connected in series with two rigid-plastic hinges. The properties of the elastic frame member shared by the two hinges should be calculated to give the desired parameters for each deformation mode. The frame member properties (L_T, A, A_S, , and G) should satisfy the following equations:

$$\frac{EI_B}{L_T}=\frac{k_v B^3 L}{12} \quad \text{(Rocking along B)} \qquad (21a)$$

$$\frac{EI_L}{L_T}=\frac{k_v L^3 B}{12} \quad \text{(For Rocking along L)} \qquad (21b)$$

$$\frac{EA}{L_T}=k_v A_F \qquad (22)$$

$$\frac{GA_{S(B)}}{L_T}=K_{H(B)} \quad \text{(Translating along } B\text{)} \qquad (23a)$$

$$\frac{GA_{S(L)}}{L_T}=K_{H(L)} \quad \text{(Translating along } L\text{)} \qquad (23b)$$

Given the stiffness values k_v and K_H, the following procedure is used to obtain the member properties: the minimum possible length L_T is used; the ratio I/A (where I and A are the member's moment of inertia and cross-sectional area) is calculated by solving Eqs. 21 and 22. An appropriate value for A is assumed (e.g. 1.0), and the corresponding moments of inertia I_B and I_L are calculated; E and G are calculated using either Eq. 21 or 22 and assuming an appropriate value for ν (e.g. 0.3). The shear areas ($A_{S(B)}$) and ($A_{S(L)}$) for shear deformation along B and L are then calculated from Eq. 23.

For a square footing subjected to biaxial loading conditions and assuming uniform bearing pressure on the foundation soil, the bounding surface for the footing horizontal capacity can be represented by a circle with radius equal to the footing horizontal capacity, as shown in Figure 9. For rectangular footings, the bounding surface is an ellipse with minor and major radii equal to the footing horizontal capacity along B and L, respectively. The equation for the bounding surface of the footing horizontal capacity in case of biaxial horizontal loading can therefore be described using an elliptical equation, i.e. (El Ganainy and El Naggar, 2009):

$$\left(\frac{V_B}{V_{Bn}}\right)^2 + \left(\frac{V_L}{V_{Ln}}\right)^2 = 1.0 \tag{24}$$

where V_B, V_L : footing horizontal load capacity along B and L, for biaxial loading, and V_{Bn}, V_{Ln} for uniaxial horizontal loading (calculated assuming a constant vertical load).

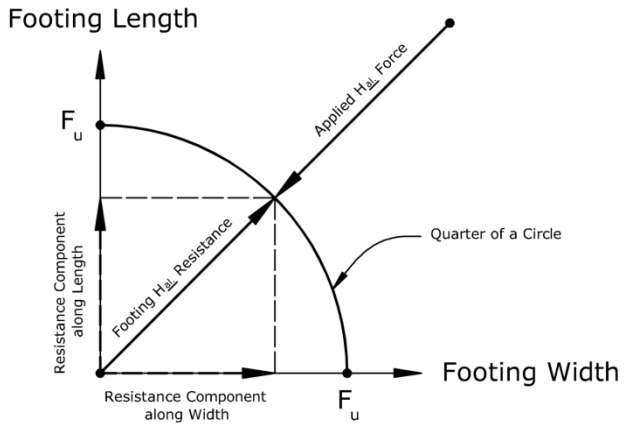

Figure 9. Graphical representation of square footings horizontal capacity components along its width and length

SOIL-FOUNDATION-STRUCTURE INTERACTION EXAMPLES

TRISEE Large-Scale 1-g Experiments

Test Description: The footing was 1 m square steel plate with concrete interface placed on a layer of saturated Ticino sand (uniform coarse-to-medium silica sand with constant volume frictional angle, φ'_{cv} = 35°, Negro et al., 1998). The sand was contained in a stiff concrete caisson with dimensions 4.6 m x 4.6 m x 3 m. The footing was embedded 1 m, with a steel formwork placed around the footing to retain the soil, and thus the sides were not in contact with soil. Two series of tests were performed on soil samples of different relative density, D_r = 85% (HD) and 45% (LD).

Vertical static loads of 100 kN and 280 kN were applied in the LD and HD tests, respectively. The footings were not loaded to failure and the BC could not be determined from the test. Lateral testing comprised of three phases: Phase I – the application of small-amplitude force-controlled cycles; Phase II – the application of an earthquake time-history; and Phase III – the application of sinusoidal displacement cycles of increasing amplitude. Only Phase III is considered in this study. The different loading phases were conducted in succession with the same experimental setup, which means the soil was loaded above the initial imposed static load before the Phase III cyclic loading commenced. Thus, it could be described as partially over-consolidated. Loading was applied in the north-south direction with an actuator at a height of 0.9 m and 0.935 m above the foundation, for the HD and LD cases, respectively.

Model Description and Parameter Estimation: The footing was modeled in the north-south direction (stiffness and BC distribution functions integrated in east-west direction). The input parameters of the cyclic curve for the vertical springs are presented in Table 2. The backbone curve was derived by extending the loading curve with a line segment tangent at its endpoint, and the stiffness of its third segment was assigned as 5% of the initial stiffness. The unload stiffness multiplier, δ_{unl} (relating unloading stiffness to loading stiffness) was estimated from the unload-reload loops to be 1.5. The vertical springs'spacing in the middle zone was twice the spacing in the edge zone.

Two cases of the direct reload curve were investigated: Case (1) with $\lambda_f = \lambda_s = 0$ and $\Lambda = 0$ (representing full gap created as a result of uplift); Case (2) models the phenomenon of "soil-squeeze-out". This occurs when lateral soil movements occur under asymmetric loading, resulting in soil heave and soil expulsion near the edge (Knappet et al., 2006), as observed in the TRISEE experiments (Negro et al., 2000). To model this behavior, the following values are used: $\Lambda = 0.1$; $\lambda_f = 0.8\zeta_{xb}^4$ with $\lambda_s = 1$, where $-1 \le \zeta_{xb} \le 1$ represents the distance of a given spring from the center of the foundation. In this case, the form of cyclic curve for springs in the mid-portion of the foundation is similar to Case (1), and those at the outer potions have low-stiffness. The FS for the HD case was assumed to be 5, and for the LD case was taken to range between 2.0-2.85. The horizontal spring was modeled using a Ramberg-Osgood (RO) hysteretic model (SeismoStruct, 2003). Its parameters (given in Table 2) are: ultimate horizontal force, H_u; horizontal yield force, H_y; initial stiffness, K_H; and the RO model curve parameter, r_o.

Table 2: Best-estimate parameters for TRISEE large-scale experiments

	HD	LD
k_{v_av} (MN/m^3)	280	100
q_{u_av} (kN/m^2)	1500	285/220
K_H (MN/m)*	100	40
H_y (kN)	70	22.5
r_o	3	6
Curve parameters		
p_1^+	0.15	0.7
p_2^+	0.85	0.9
α_2	0.7	1
α_3	0.05	0.05
δ_{unl}	1.5	1.5
λ_f / Λ		
(1) λ_s =0	0 / 0	0 / 0
(2) λ_s =1	$0.8\zeta_{xb}^4$ / 0.1	$0.8\zeta_{xb}^4$ / 0.1

$^+$ ratio of the ultimate load ; * represents the case $K_H = 0.4K_V$

Computed Responses Using Generalized Dynamic BNWF Model: **HD Case:** The calculated and measured responses for the HD case are in good agreement as shown in Fig. 10. In particular, the model's ability to capture the characteristic S-shaped moment-rotation response is noted. However, the energy dissipated (enclosed area) in the moment-rotation loops was different for cases (1) and (2). This clearly shows the importance of considering "soil-squeeze-out" for predicting the moment-rotation response; otherwise the damping present in the system could be considerably underestimated. Also, the measured and predicted horizontal force-displacement responses are in good agreement. The maximum settlement was reasonably predicted, with calculated and measured values of 21 mm and 19 mm. Unlike the measured response, the computed horizontal force-displacement response showed some permanent displacement, which was sensitive to variations in the horizontal spring parameters (i.e. significant variations in the parameters changed the response mode).

LD Case: Table 3 shows the moment capacities for the no-sliding case to be larger than the sliding-allowed case, reflecting the effect of coupling between the horizontal and rotational-vertical responses. The computed response was sensitive to the horizontal resistance, e.g., larger values of H_y resulted in more rotation (and larger settlement) while smaller values resulted in more sliding. Figure 11 shows the moment-rotation and horizontal force-displacement responses obtained for three different H_y cases. The results for the best-estimate case are laterally shifted from the measured response, and displayed a permanent negative rotation but not displacement. Also, the moment-rotation responses of the best-estimate and no-sliding cases are similar (i.e. rotation dominated the deformation mode for both cases). In contrast, for smaller H_y (sliding-dominant case), permanent negative displacements, not rotations, are predicted. This shows that the problem is highly coupled, and that inadequate coupling between the vertical-rotational and horizontal responses can lead to poor predictions, especially for permanent horizontal displacements. The degree of coupling between the horizontal and rotation-vertical responses could be enhanced by employing distributed coupled normal-tangential nonlinear Winkler models (e.g. Allotey and Foschi, 2005). The computed moment-rotation response displayed some form of S-shaping, especially for case (1) as shown in Fig. 14a. Case (2) agrees better with the measured response and shows the importance of considering "soil-squeeze-out". Fig. 14c shows that the predicted maximum settlement is about the same as the measured settlement.

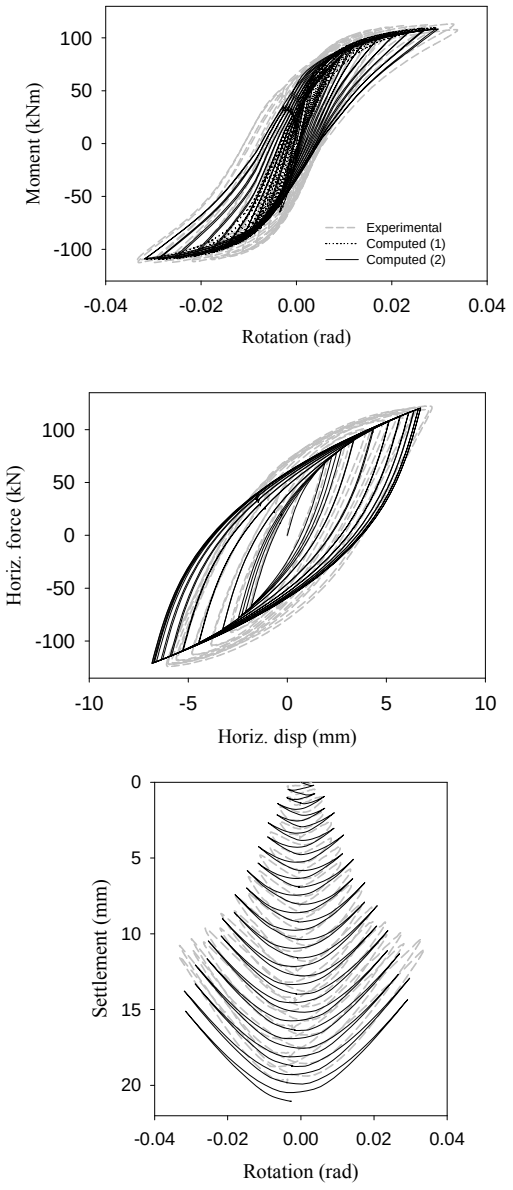

Figure 10: Experimental and computed responses for HD test: a) moment-rotation; b) horizontal force-displacement; c) settlement-rotation

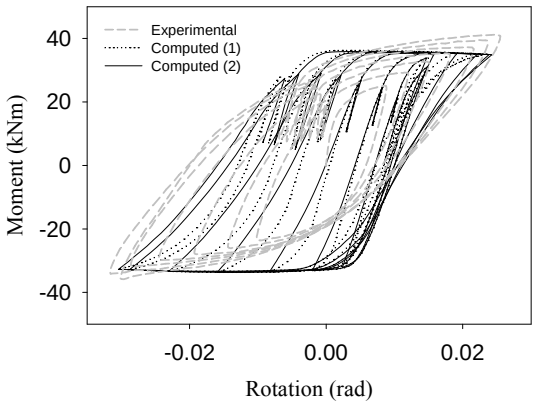

a)

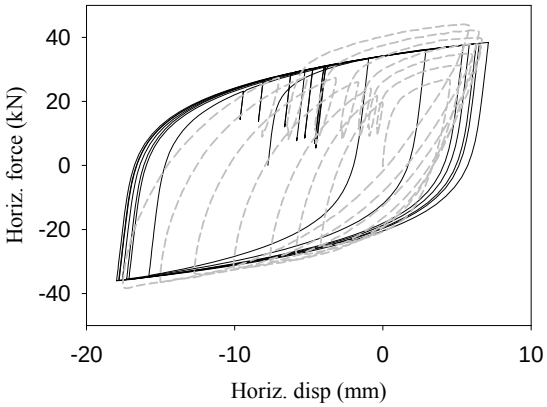

b)

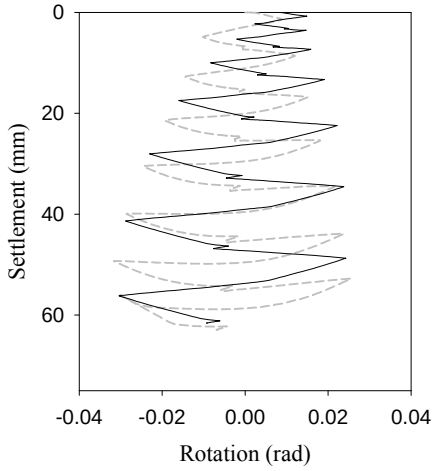

c)

Figure 11: Experimental and adjusted computed responses for LD test: a) moment-rotation; b) horizontal force-displacement; c) settlement-rotation

Table 3: LD moment and horizontal force capacities of different stiffness and BC distributions

	Stiffness/BC distribution			
Stiffness BC	Uniform* Uniform*		Concave+ Convex#	
FS	2.85	2.2	2.85	2.2
Sliding allowed				
Max horiz. force (kN)	32.98	27.22	42.97	38.45
Max. moment (kNm)	30.81	25.45	38.95	35.95
Sliding disallowed				
Max horiz. force (kN)	34.39	28.77	45.75	39.04
Max. moment (kNm)	32.15	26.90	42.78	36.46

+ Edge stress factor = 0.65, curve shape factor = 2;
# Edge stress factor = 6, curve shape factor = 2

Computed Response Using the Coupled BNWF Model:

The actual moment-rotation relation of the rectangular footing was calculated using the soil properties given in Table 2. The corresponding moment-curvature relation of the curvature hinge was calculated by dividing the rotation values by the tributary length of the hinge. This relation was approximated by a trilinear moment-curvature relation and was assigned to the curvature hinge. The slope of the elastic branch of the bilinear shear force-shear displacement relation of the shear hinge assembly was given by K_H. The footing horizontal capacity, F_U, was calculated as the vertical load acting on the footing (300 kN and 100 kN for the HD and LD tests) multiplied by the friction coefficient between the footing base and soil, $0.6\tan(\phi'_{cv})$.

The horizontal yield force, H_y, was taken as above and the shear displacement corresponding to the footing horizontal yield capacity was obtained by fitting the experimental horizontal force-displacement hysteresis loops for the HD and LD tests with the hysteresis loops obtained from Perform-3D. A value of 5 mm and 4 mm for the HD and LD tests, respectively, was found to give a good fit. It should be noted that bilinear approximation should be sufficient for modeling the footing behavior of real buildings. Hence, the elastic horizontal stiffness of the footing, K_H, and its horizontal capacity, F_U, will be the only parameters required to define the shear force-shear displacement relation of the footing.

Figures 12 compares the experimental and numerical hysteretic moment-rotation curves for the HD and LD tests, and Figure 13 compares their hysteretic horizontal force-displacement curves. In general, the agreement between the two sets is good, verifying the ability of the proposed approach to simulate shallow foundations behavior. It should be noted that the numerical curves slightly overestimate the hysteretic.

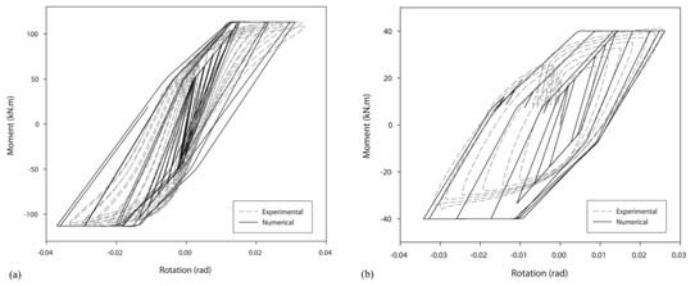

Figure 12. Experimental and numerical hysteretic moment-rotation curves, a) for HD test; b) for LD test

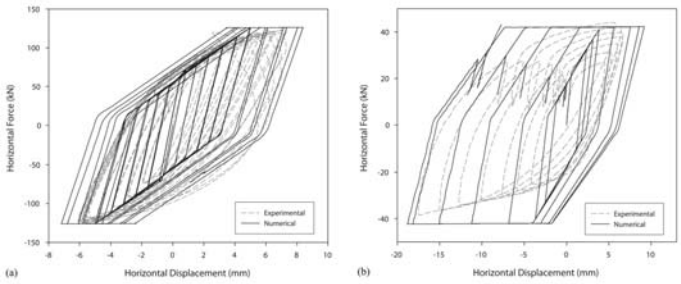

Figure 13. Experimental and numerical hysteretic horizontal force-displacement curves, a) for HD test; b) for LD test

The SSG02 Centrifuge Experiment

Experimental Setup:

The SSG02 centrifuge experiment was conducted at the centrifuge facility of the University of California, Davis. It was part of a larger SFSI project involving the testing of several SFSI systems. The test considered in this study is a slow-cyclic horizontal test conducted at Station B on the test bed (Fig. 14). The structure was a 10 m wall supported by a 2.67 m x 0.69 m spread footing (all prototype units) with a structural weight of 280 kN. The load was applied in the lengthwise direction of the wall at a distance of 4.9 m above the base. The input displacement history was harmonic with a maximum displacement of 310 mm. The underlying soil bed was 200 mm thick composed of dry Nevada sand with an average relative density of 80% and its frictional angle was 42°(Gajan et al., 2003).

Model description and parameter estimation: The foundation was modeled in the lengthwise direction with stiffness and bearing capacity (BC) distribution functions integrated in the orthogonal direction. Fifty-one vertical springs were used, and one horizontal spring (attached to the center node). The springs spacing in the middle zone was twice the spacing in the edge zone. The vertical springs were modeled using the presented BNWF model, whereas the RO hysteretic model was used to represent the horizontal spring. Since the soil was non-weakening, cyclic degradation was not accounted for.

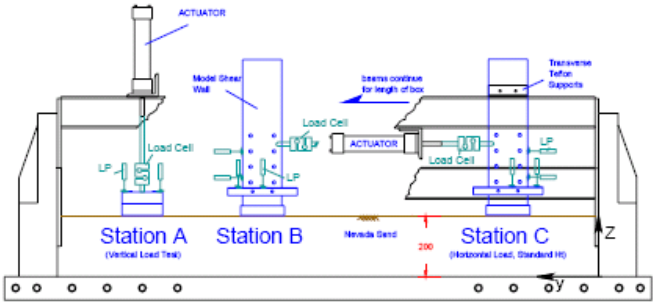

Figure 14: Side view of model container with selected wall-footing locations and typical instrument locations for SSG02 slow-cyclic tests (after Gajan et al., 2003)

The stiffness and BC were assumed uniformly distributed for both tests. The BC was estimated from an initial vertical load-deformation test conducted to failure at Station A, and was found to be 1920 kN, implying FS = 6.8. Using the vertical load-deformation curve, the loading curve parameters were obtained from the unload-reload and the backbone curves of the vertical load test. The unload stiffness multiplier that relates the stiffness of the unload curve to the backbone curves, δ_{unl}, was estimated to be 3. The cyclic curve shape parameter Λ was taken as 0.1. Also, two cases were chosen for the cyclic curve shape parameters λ_s and λ_f: Case (1) refers to the traversal of the full gap distance developed as a result of foundation uplift; and Case (2) refers to the phenomenon of "soil squeeze out" due to asymmetric loading (Allotey and El Naggar, 2008b). The initial stiffness of the horizontal spring was taken as half of the elastic half-space recommended stiffness ($0.4K_V$) as noted from other case studies. The relevant input parameters are presented in Table 4.

Table 4: Vertical and horizontal springs model parameters

Vertical	
Stiffness/BC distribution parameters	
$k_{v\ av}$ (MN/m^3)	200
$q_{u\ av}$ (kN/m^2)	980
Stiff. dist.	Uniform
BC dist.	Uniform
Curve parameters	
p_1^*	0.05
p_2^*	0.8
α_2	0.3
α_3	0.03
δ_{unl}	3
Λ	0.1
λ_f (λ_s=1)(1)	0
(2)	$0.8\xi_r^4$
Horizontal	
K_H (MN/m)	80$^+$
r_o	15
P_{yH} (kN)	70

* ratio of ultimate load; $^+$ represents the case $K_H = 0.4K_V$

Results and discussion: Figure 15a shows the moment-rotation response not including $P-\delta$ effects; and Fig. 15b shows the results including the $P-\delta$ effects. It is noted that the computed response including the $P-\delta$ effects is in good agreement with the measured response. The results presented are for Case (2), which as noted before, predicts the moment-rotation response more accurately. Also, measured and computed responses display a strain-softening response at larger rotations due to the P-δ effect on the response. It is therefore important that secondary order P-δ effects be duly considered in SFSI analysis.

Figure 16a compares the measured and predicted horizontal force-displacement responses. The cyclic horizontal displacements are well predicted, however, permanent horizontal displacements are not. This is attributed to the limited coupling between the vertical-rotation and horizontal responses (Allotey and El Naggar, 2008b). This can be improved by enhancing the coupling between both response modes as in Allotey and Foschi (2005). It is noted from Fig. 16b that the general settlement pattern is well predicted, however, the final settlement is under-predicted by about 10 mm. This represents an improvement on the macro-element prediction of Gajan et al. (2005).

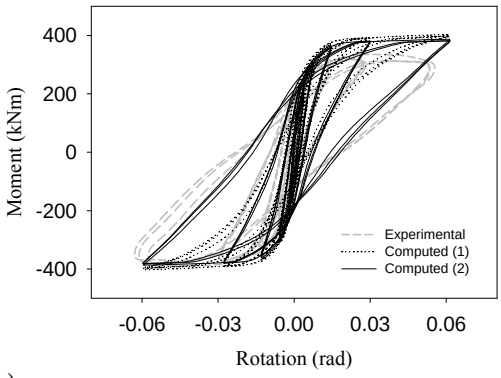

a)

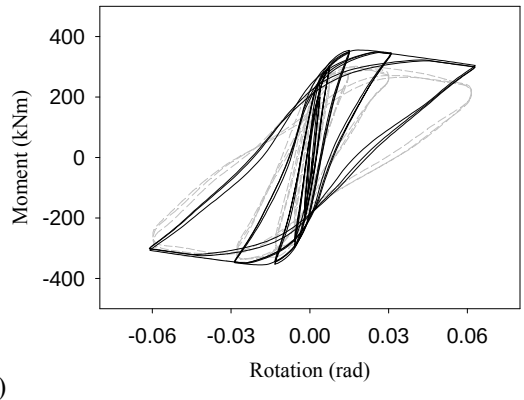

b)

Figure 15:Experimental and computed results for SSG02 Station B test: a) moment-rotation response with no P-delta; b) moment-rotation response with P-delta

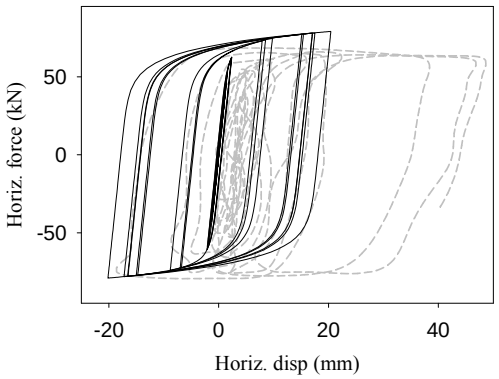

a)

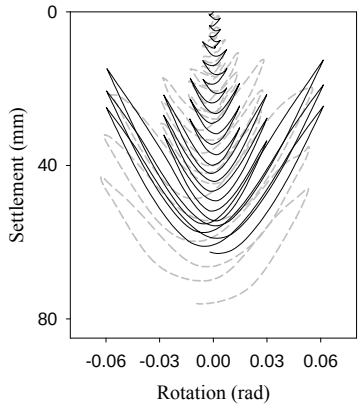

b)

Figure 16: Experimental and computed results for SSG02 Station B test: a) horizontal force-displacement response; b) settlement-rotation response

ACKNOWLEDGEMENT

The author would like to acknowledge the contributions of his former students: Dr. Nii Allotey and Mr. Hesham El Ganainy. The presented work cannot be completed without their intellectual contributions, hard work and dedication.

REFERENCES

Allotey, N. and El Naggar, M.H. [2003]. Analytical moment-rotation curves for rigid foundations based on a Winkler model. Soil Dyn. and Earthquake Engrg., 23(5), pp. 367-381.

Allotey, N. and El Naggar, M.H. [2005]. Soil-structure interaction in performance-based design – a review. Proc. of 11th IACMAG, Torino, June 19-24, vol. 3, pp. 595-602.

Allotey, N. and El Naggar, M.H., [2006]. Cyclic degradation/hardening models in total stress analysis: new equations. 1s^{t} Euro. Conf. on Earthquake Engrg. and Seismology (a joint event of the 13th ECEE & 30th General Assembly of ESC), Paper No. 1015, Geneva.

Allotey, N. and El Naggar, M. H. [2007]. Modeling of cyclic response of shallow foundations with Winkler model: some issues. Proceedings of 9th Canadian Conference on Earthquake Engineering, Ottawa, June 25, Paper no. 1156.

Allotey, N. and El Naggar, M.H. [2008a]. Generalized Dynamic Winkler model for nonlinear soil-structure interaction analysis. Canadian Geotechnical J., Vol. 45, No. 4, pp. 560-573.

Allotey, N. and El Naggar, M.H. [2008b]. An investigation into the Winkler modeling of the cyclic response of rigid footings. Soil Dynamics and Earthquake Engineering, Vol. 28, No. 1, pp. 44-57.

Allotey, N. and El Naggar, M.H. [2008c]. A consistent soil fatigue framework based on the number of equivalent cycles. J. of Geotech. and Geol.Engrg., Vol. 26, No. 1, pp. 65-77.

Allotey, N. K. and Foschi, R. O. [2005]. Coupled *p-y t-z* analysis of single piles in cohesionless soil under vertical and/or horizontal ground motion. J. of Earthquake Engineering, Vol. 9, no. 6, pp.755-776.

American Society of Civil Engineers (ASCE), [2000]. FEMA-356 -Prestandard and commentary for the seismic rehabilitation of buildings, Washington, DC.

Andersen, K. H., Kleven, A. and Heine, D. [1988]. Cyclic soil data for design of gravity structures. J. of Geotechnical Engineering, ASCE, Vol. 114, no. 5, pp. 517-539.

Anderson, D. L. [2003]. Effect of foundation rocking on the seismic response of shear walls. Canadian Journal of Civil Engineering, Vol. 30, pp. 360-365.

Anthes, R. J. [1997]. Modified rainflow counting keeping the load sequence. Intl. J. of Fatigue. Vol. 19, no. 7, pp. 529-535.

Applied Technology Council (ATC) [1996]. ATC 40 - The seismic evaluation and retrofit of concrete buildings, Vol. I & II, Redwood, California.

Auvinet, G., and Mendoza, M. J. [1986]. Comportamiento de diversos tipos de cimentacion en la zone lascustre de la Ciudad de Mexico durante el sismo del 19 septiembre de 1985. Proc., symposium-Los Sismos de 1985: casos deMecanica de Suelos, Mexico (in Spanish).

Aviles, J. and Perez-Rocha L. E. [2003]. Soil-structure interaction in yielding systems. Earthquake Engineering and Structural Dynamics, Vol. 32, pp. 1749-1771.

Badoni, D.and Makris, N. [1996]. Nonlinear response of single piles under lateral inertial and seismic loads. Soil Dynamics and Earthquake Engineering, Vol. 15, pp. 29-43.

Boulanger, R. W., Curras, J. C., Kutter, B. L., Wilson, D. W. and Abghari, A. [1999]. Seismic soil-pile-structure interaction experiments and analysis. J. of Geotech. and Geoenviro. Engineering, ASCE, Vol. 125, No. 9, pp. 750-759.

Building Seismic Safety Council (BSSC) [1997a]. FEMA 273/274 - NERHP Guidelines for the Seismic Rehabilitation of Buildings, Vol. I – Guidelines, Vol. II – Commentary, Washington.

Building Seismic Safety Council (BSSC) [1997b]. FEMA 302/303 - NEHRP recommended provisions for seismic regulations for new buildings and other structures, Vol. I – Guidelines, Vol. II – Commentary, Building Seismic Safety Council, Washington DC.

Calvi, G. M. [2004]. Recent experience and innovative approaches in design and assessment of bridges. Proceedings of 13th World Conference on Earthquake Engineering, Vancouver, Paper no. 5009.

Carr, A. J. [2001]. Ruaumoko 3D - User's Manual, University of Canterbury, Christchurch, New Zealand.

Carter, J. P., Booker, J. R. and Wroth, C. P. [1982]. A critical state soil model for cyclic loading. Soil Mechanics – Transient and Cyclic Loads, Eds. G. N. Pande and O. C. Zienkiewicz, pp. 219-252, John Wiley & Sons.

Cassidy, M. J., Byrne, B. W. and Randolph, M. F. [2004]. A comparison of the combined load behaviour of spudcan and caisson foundations on soft normally consolidated clay. Geotechnique, Vol. 54, no. 2, pp 91-106.

Celebi, M. and Crouse, C. B. [2001]. Recommendations for soil structure interaction (SSI) instrumentation, Report for Consortium of Organizations for Strong-motion Observation Systems, Emeryville, CA.

Chatzigogos, C.T., Pecker, A. and Salencon, J. [2009]. Macroelement modeling of shallow foundations. Soil Dynamics and Earthquake Engineering, Vol. 29, pp. 765-781.

Chopra, A. K. and Yim, C. S. [1984]. Earthquake responses of structures with partial uplift on Winkler foundation. Earthq. Engrg. and Struct. Dynamics, Vol. 12, pp. 265-281.

Comartin, C. D., Keaton, J. R., Grant, P. W., Martin, G. R., Power, M. S. [1996]. Transitions in seismic analysis and design procedures for buildings and their foundations. Proc. 6th Workshop on the Improvement of Structural Design and Construction Practice in the US and Japan, Victoria, BC, ATC Report No. ATC 15-5.

Cremer, C., Pecker, A., and Davenne, L. [2001]. Cyclic macro-element for soil-structure interaction: Material and geometrical non-linearities. Int. J. Numer. Anal. Methods Geomech., 25(13), 1257-1284.

Crouse, C. B. and Mcguire, J. [2001]. Energy dissipation in soil-structure interaction. Earthq. Spectra, 17(2), pp. 235-259.

CSI 2002. SAP2000 Version 8.0 Nonlinear – User's Manual, Computers and Structures Inc., Berkeley, CA.

De Alba, P., Seed, H. B. and Chan, C. K. [1976]. Sand liquefaction in large-scale simple shear tests. J. of Geotech. Engrg. Division, ASCE, 102, GT9, 909-927.

Eguchi, R. T., Goltz, J. D., Taylor, C. E., Chang, S. E., Flores, P. J., Johnson, L. A., Seligson, H. A. and Blais, N. C. [1998]. Direct economic losses in the Northridge earthquake: a three-year post-event perspective. Earthquake Spectra, Vol. 14, pp. 245-264.

El Ganainy, H. and El Naggar, M. H. [2009]. Efficient 3D nonlinear Winkler model for shallow foundations. Soil Dynamics and Earthquake Engineering, Vol. 29, No. 8, pp. 1236-1248.

El Naggar, M.H. and Bentley, K.J., [2000]. Dynamic analysis for laterally loaded piles and dynamic p-y curves. Canadian Geotechnical J., Vol. 37, No. 6, pp. 1166-1183.

El Naggar, M.H. and Novak, M. [1996]. Nonlinear analysis for dynamic lateral pile response. Soil Dynamics and Earthquake Engineering, Vol. 15, No. 4, pp. 233-244.

El Naggar, M.H. and Novak, M. [1994]. Non-linear model for dynamic axial pile response. J. of Geotechnical Engineering, ASCE, Vol. 120, No. 2, February, pp. 308-329.

El Naggar, M. H., Novak, M., Sheta, M., El-Hifnawy, L., El-Marsafawi, H., and Ramadan, O., [2007]. DYNA5, ver. 5.4. a computer program for calculation of foundation response to dynamic loads. Geotechnical Research Centre, The University of Western Ontario, London, Ontario

El Naggar, M.H., Shayanfar, M.A., Kimiaei, M., and Aghakouchak, A.A. [2005]. Simplified BNWF model for nonlinear seismic response analysis of offshore piles. Canadian Geotechnical J., Vol. 42, No. 2, pp. 365-380.

El-Tawil, S. and Deierlein, G. G. [2001]. Nonlinear analysis of mixed steel-concrete frames II: Implementation and verification. J. of Structural Engineering, 127(6), 656-665

Federal Emergency Management Agency (FEMA), [2004]. FEMA 440 – Improvements to inelastic seismic analysis procedures, Washington, DC.

Filiatrault, A., Anderson, D. L. and DeVall, R. H. [1992]. Effect of weak foundation on the seismic response of core wall type buildings. Can. J. of Civil Engrg., Vol. 19, pp. 530-539.

Finn, W. D. L. [2005]. A study of piles during earthquakes: issues of design and analysis. Bulletin of Earthquake Engineering, Vol. 3, pp. 141-234.

Gajan. S., Phalen. J. D. and Kutter. B. L. [2003]. Soil-foundation-structure interaction: shallow foundations. Centrifuge Data Report for SSG02, Report no. UCD/CGMDR-03/01, Center for Geotechnical Modeling, University of California, Davis.

Gajan, S., Thomas, J. M., and Kutter, B. L. [2005]. Physical and analytical modeling of cyclic load-deformation behavior of shallow foundations. Proc. of 57th Annual Meeting of Earthquake Engineering Research Institute, Mexico.

Gazetas, G. [1991]. Formulas and charts for impedance of surface and embedded foundations. J. of Geotech. Engrg., ASCE, Vol. 117, no. 9, pp. 1363-1381.

Gazetas, G. [2001]. SSI issues in two European projects and a recent earthquake. Proc. of 2nd UJNR Workshop on Soil-Structure Interaction, Tsukuba, Japan.

Gazetas, G. and Dobry, R. [1984]. Simple radiation damping model for piles and footings. J. of Engrg. Mechanics, ASCE, 110(6), pp. 937-956.

Gazetas, G., and Mylonakis, G. [1998]. Seismic soil-structure interaction: new evidence and emerging issues. Geotech. Earthquake Engrg. and Soil Dyn.-III, ASCE Geotech. Special Publication no. 75, Eds. P. Dakoulas, M. Yegian, and R. D. Holtz, pp. 1119-1174.

Gazetas, G. and Mylonakis, G. [2001]. Soil structure interaction effects on elastic and inelastic structures, Proc. 4th Int. Conf. on Rec. Advances in Geotech. Earthquake Engrg. and Soil Dyn., San Diego, CA, Paper. No. SOAP-2.

Gerolymos, N. and Gazetas, G. [2005]. Phenomenological model applied to inelastic response of soil-pile interaction systems. *Soils and Foundations*, Vol. 45, no. 4, pp. 119-132.

HCItasca [2002]. *FLAC* 3D Version 2.1 - User's Manual, HCItasca Consulting, Minneapolis, MN.

Houlsby, G. T., and Cassidy, M. J. [2002]. A plasticity model for the behavior of footings on sand under combined loading. Geotechnique, Vol. 52, No. 2, pp. 117-129.

Housner, G. W. [1963]. Behavior of inverted pendulum structures during earthquakes. Seismological Society of America - Bulletin, Vol. 53, No. 2, pp. 403-417.

Hyodo, M., Yamamoto, Y. and Sugyiama, M. [1994]. Undrained cyclic shear behaviour of normally consolidated clay subjected to initial static shear stresses. Soils and Foundations, Vol. 34, no. 4, pp. 1-11.

Idriss, I. Z., Dobry, R.and Singh, R. D. [1978]. Nonlinear behaviour of soft clays during cyclic loading. J. of Geotech. Engineering, ASCE, Vol. 104, GT12, pp. 1427-1447.

Iguchi, M. [2001]. On effective input motions: observations and simulation analysis. Proceedings of 2nd UJNR Workshop on Soil-Structure Interaction, Tsukuba, Japan.

Kerr, A. D. [1989]. Tests and analysis of footings on a sand base. Soils and Foundations, Vol. 29, no. 3, pp. 83-94.

Knappet, J. A., Haigh, S. K. and Madabhushi, S. P. G. [2006]. Mechanisms of failure for shallow foundations under earthquake loading. Soil Dyn. and Earthquake Engineering, Vol. 26, pp. 91-102.

Kramer, S. L. and Elgamal, A. W. [2001]. Modeling soil liquefaction hazards for performance-based earthquake engineering. PEER Rep. no. 2001/13, University of California, Berkeley, CA.

Kurimoto, O. and Iguchi, M. [1995]. Evaluation of foundation input motion based on observed seismic waves. J. of Struct. Construction Engrg. (in Japanese), Vol. 472, pp. 67-74.

Li, K. [2002]. CANNY Version C02, Technical and User's Manual, CANNY Structural Analysis Ltd., Vancouver, BC.

Long, J. H. and Vanneste, G. [1994]. Effects of cyclic lateral loads on piles in sands. Journal of Geotechnical Engineering, ASCE, Vol. 120, no. 1, pp. 225-243.

Maugeri, M., Musumeci, G., Novita, D. and Taylor, C. A. [2000]. Shaking table test of failure of a shallow foundation subjected to an eccentric load. Soil Dyn. and Earthquake Engineering, Vol. 20, pp. 435-444.

Moehle, J. and Deierlein, G. [2004]. A framework methodology for performance-based earthquake engineering. Proc. of 13th World Conference on Earthquake Engineering, Paper no. 679, Vancouver, BC.

Negro, P., Paolucci, R., Pedretti, S. and Faccioli, E. [2000]. Large scale soil-structure interaction experiments on sand under cyclic load. Proc. of 12th World Conf. on Earthquake Engineering, Paper no. 1191, Auckland, New Zealand.

Nogami, T. and Chen, H. S. [2004]. Formulation of dynamic soil stiffness for shallow foundations by differential equation cell method. Proc. of 11th ICSDEE/3rd ICEGE, Berkeley, CA, pp. 88-95.

Novak, M., Nogami, T. and Aboul-Ella, F. [1978]. Dynamic soil reactions for plane strain case. J. of Engineering Mechanics Division, ASCE, Vol. 104, no. 4 pp. 953-959.

Pacific Earthquake Engineering Research Center (PEER), [2000]. The Open System for Earthquake Engineering Simulation (OpenSees) [http://opensees .berkeley.edu].

Pecker, A. [1997]. Analytic formulae for the seismic bearing capacity of shallow strip foundations. Seismic Behaviour of Ground and Geotechnical Structures, Ed. S. Pinto, A. A. Balkema, Rotterdam, pp. 261-268.

Pecker, A. and Pender, M. J. [2000]. Earthquake resistant design of foundations: new construction. Proc. of Intl. Conf. in Geotech. and Geol. Engrg. - GeoEng 2000, Melbourne, Australia, pp. 303-332.

Pender, M. J.and Ni, B. [2004]. Nonlinear vertical vibration characteristics of rigid foundations. Proceedings of 11th ICSDEE/3rd ICEGE, Berkeley, CA, pp. 719-725.

Popescu, R. and Prevost, J. H. [1993]. Centrifuge validation of a numerical model for dynamic soil liquefaction. Soil Dynamics and Earthquake Engineering, Vol. 12, pp. 73-90.

Prakash, V., Powell, G. H. and Campbell, S. [1993]. DRAIN-2DX: Base program description and user guide, Version, 1.10. Report UCB/SEMM-93/17, University of California, Berkeley, CA.

Priestley, M. J. N. and Park, R. [1987]. Strength and ductility of concrete bridge columns under seismic loading. ACI Structural Journal, 84(8), pp. 61-76.

Priestley, M. J. N. [2000]. Performance-based seismic design. Proc. of 12th World Conference on Earthquake Engineering, Paper no. 2831, Auckland, New Zealand.

Psycharis, I. N. and Jennings, P. C. [1984]. Rocking of slender rigid bodies allowed to uplift. Earthquake Engineering and Structural Dynamics, Vol. 11, pp. 57-76.

Pyke, R. [1979]. Nonlinear soil models for irregular cyclic loadings. J. of Geotech. Engrg., ASCE, 105, pp. 715-726.

SASSI2000 [1999]. SASSI 2000 User's Manual, SASSI 2000 Inc., Oakland, CA.

Schultze, E. [1961]. Distribution of stress distribution beneath a rigid foundation. Proc. of 5th Intl. Conf. on Soil Mechanics and Foundation Engineering, Vol. 6, pp. 807-813.

SEAOC [1995]. SEAOC Vision [2000] Performance based seismic engineering of buildings: conceptual framework, Vol. I & II, Sacramento, CA.

SeismoSoft [2003]. SeismoStruct — A computer program for static and dynamic nonlinear analysis of framed structures [Online]. Available: http://www .seismosoft.com.

Sharma, S. S. and Fahey, M. [2003]. Degradation of stiffness of cemented calcareous soil in cyclic triaxial tests. J. of Geotech. and Geoenvir. Engineering, 129(7), pp. 619-629.

Somerville, P. G. [1998]. Emerging art: earthquake ground motion. Geotech. Earthquake Engrg. and Soil Dyn. III, ASCE, eds. P. Dakoulas, M. K. Yegian, R. D. Holtz, pp. 1-38.

Stewart, J. P., Kim, S., Bielak, J., Dobry, R., Power and M. S. [2003]. Revisions to soil-structure interaction procedures in NEHRP design provisions. Earthquake Spectra, 19 (3), pp. 677-696.

Trifunac, M. D., and Todorovska, M. I. [1999]. Reduction of structural damage by nonlinear soil response. J. of Structural Engineering, 125(1), pp. 89-97.

Trifunac, M. D., Todorovska, M. I. and Hao, T. Y. [2001]. Full-scale experimental studies of soil-structure interaction – a review. Proc. of 2nd US-Japan Workshop on Soil-Structure Interaction, Tsukuba, Japan.

Valles, R. E., Reinhorn, A. M., Kunnath, S. K., Li, C. and Madan, A. [1996]. IDARC-2D Version 4.0: A program for the inelastic damage analysis of buildings. Report no. NCEER-96-0010, NCEER, University of New York, NY.

Vesic, A. S. [1973]. Analysis of ultimate loads on shallow foundations. J. of Soil Mechanics and Foundations Division, ASCE, 98(3), pp. 45-73.

Vucetic, M. and Dobry, R. [1988]. Degradation of marine clays under cyclic loading. J. of Geotech. Engrg., ASCE, 114(2), pp. 133-149.

Wang, S., Kutter, B. L., Chacko, J. M., Wilson, D. W., Boulanger, R. W., and Abghari, A. 1998. Nonlinear seismic soil-pile-structure interaction. Earthquake Spectra, 14(2), pp. 377-396.

Wolf, J. P. and Deeks, A. J. [2004]. Foundation vibration analysis: a strength-of-materials approach, Elsevier, Oxford, UK.

Wolf, J. P. and Preisig, M. [2003]. Dynamic stiffness of foundation embedded in layered half-space based on wave propagation in cones. Earthquake Engineering and Structural Dynamics, Vol. 32, pp. 1075-1098.

Wotherspoon, L. M., Pender, M. J. and Ingham, J. M. [2004]. Effects of foundation models on the earthquake response of building systems. Proc. of 11th ICSDEE/3rd ICEGE, Berkeley CA, pp. 766-773.

Zeng, X. and Steedman, R. S. [1998]. Bearing capacity of shallow foundations. Geotechnique, 48 (2), pp. 235-256.